Review of Scientific Instruments ARTICLE pubs.aip.org/aip/rsi

Table-top source for x-ray absorption spectroscopy with photon energies up to 350 eV

Cite as: Rev. Sci. Instrum. 95, 103001 (2024); doi: 10.1063/5.0219921
Submitted: 21 May 2024 • Accepted: 3 September 2024 •
Published Online: 2 October 2024

O. A. Naranjo-Montoya, M. Bridger, R. Bhar, L. Kalkhoff, M. Schleberger, H. Wende, A. Tarasevitch,[a] and U. Bovensiepen

AFFILIATIONS

Faculty of Physics and Center for Nanointegration (CENIDE), University of Duisburg-Essen, Lotharstrasse 1, 47057 Duisburg, Germany

[a]Author to whom correspondence should be addressed: alexander.tarasevitch@uni-due.de

ABSTRACT

We present a table-top setup for x-ray absorption spectroscopy (XAS) based on high harmonic generation (HHG) in noble gases. Using sub-millijoule pump pulses at a central wavelength of 1550 nm, broadband HHG in the range of 70–350 eV was demonstrated. The HHG coherence lengths of several millimeters were achieved by reaching the nonadiabatic regime of harmonic generation. Near edge x-ray absorption fine structure spectroscopy experiments on the boron K edge of a boron foil and a hexagonal boron nitride (hBN) 2D material demonstrate the capabilities of the setup. Femtosecond pulse duration makes pump–probe XAS experiments with corresponding time resolution possible.

I. INTRODUCTION

Soft x-ray spectroscopy is a well-established methodology that comprises various photon-in photon-out techniques to probe core level excitations of atoms, molecules, and condensed matter. X-ray absorption spectroscopy analyzes the transition from a core level to an unoccupied state, and x-ray emission detects the x-ray fluorescence induced by the creation of a core hole. While both techniques provide information on the excited core levels, they complement each other regarding the valence electronic states. X-ray absorption probes the unoccupied and x-ray emission probes the occupied valence electronic structure.[1]

In the spectral range near the resonant core level excitation element and orbital selective insights into the unoccupied valence electronic structure are obtained primarily in near edge x-ray absorption fine structure (NEXAFS).[1,2] In the extended spectral range, the locally emitted photoelectron wave function upon resonant core level excitation is scattered back from the neighboring ion cores in molecules and condensed matter, which leads to interference effects in the absorption cross section detected in extended x-ray absorption fine structure absorption spectroscopy (EXAFS). This technique analyzes the local ion core structure.[3]

More recently, resonant inelastic x-ray scattering (RIXS) has become available as a tool to measure low energy excitations and their dispersion relation in momentum space.[4,5]

Clearly, x-ray spectroscopy is a very important tool in various fields of the natural sciences, such as, e.g., material science,[6–8] interface science,[9] coordination chemistry,[10] energy conversion and catalysis,[11] photosynthesis,[12] and biology.[13] Moreover, it is widely used in the conservation of cultural heritage and art.[14,15]

A major effort in setting up an x-ray spectrometer is dedicated to the x-ray source. Early efforts exploited the emission of x-ray tubes.[16,17] The required spectral resolution and signal to noise ratio lead to very long times needed for data accumulation in such laboratory-based instruments. The high brilliance provided by synchrotron light sources resulted in considerable improvement in this regard, and at the present time most x-ray spectroscopy experiments are conducted at synchrotron light sources.[18] Higher x-ray photon fluxes and shorter pulse durations became possible after having shifted from storage rings used in synchrotron light sources to linear accelerators in x-ray free electron lasers, which provide dedicated instruments for soft x-ray spectroscopy.[19–22] This development also provides interesting opportunities for non-linear x-ray spectroscopy.[23,24]

The limited access to the necessary beam times has always fueled the development of table-top x-ray light sources, and laser-based approaches have led to considerable success. Essentially,

two mechanisms of light–matter interaction are exploited. For table-top x-ray spectroscopy, light sources based on laser plasma generation[25,26] and high harmonic generation (HHG) in gases[27–33] have been developed. Such laser-based sources allow the generation of ultrashort x-ray pulses,[34–41] which provide highly relevant opportunities for pump–probe experiments and time domain x-ray spectroscopy.[42–44] The plasma-based approach provides sufficient photon flux also at hard x-ray photon energies. HHG allows shorter pulse durations[44] reaching the attosecond limit, a development that was recognized by awarding the Nobel Prize in Physics 2023 to Agostini, L'Huillier, and Krausz.

Using mid-infrared femtosecond pump pulses, HHG with photon energies exceeding 1 keV became available,[27,45] and for competing with the accelerator-based sources in terms of the x-ray photon yield, a phase matched harmonic emission from a larger atomic ensemble became essential. The phase matched HHG by adjusting the gas pressure in the interaction volume has been discussed and demonstrated for HHG in gas jets,[29,46–50] in hollow core waveguides (HCWs)[39,40,45,51–55] or both,[56] in hollow core fibers or tubes in transverse geometry,[30,31,33,57] and in gas cells.[32,58,59] The advantage of HCWs in longitudinal geometry is that they allow phase matched emission at potentially higher gas pressures and/or on longer distances, which can be more promising from the standpoint of the photon yield. Important limitations, in this case, are absorption[56] and the necessity to keep the gas pressure in the HCW constant along the capillary to provide a long coherence length of the HHG.

For the phase matching, two types of phase contributions have to be taken into account: time independent (neutral gas dispersion and geometrical contribution) and time dependent (plasma dispersion and nonlinear refraction). The time dependent one comes into play at higher pump intensities, and the HHG switches correspondingly from adiabatic to nonadiabatic[37,46,60] (or time gated[55]) regimes.

In this paper, we demonstrate a table-top x-ray source based on HHG in noble gases using low energy (compared to Refs. 27 and 45) pump pulses at a wavelength of 1550 nm. The generated x-ray pulses were applied to the measurements of the x-ray absorption spectra (XAS) on the boron K-edge. We show that switching to the nonadiabatic regime is essential for the phase matched harmonic emission.

II. EXPERIMENTAL SET-UP

The pump laser for the HHG was an upgraded version of the 100 Hz optical parametric chirped pulse amplification (OPCPA) setup reported in Ref. 61. The setup occupied six 2400×1200 mm^2 optical tables, and its schematic is depicted in Fig. 1. The system was seeded by a Ti:sapphire (Ti:Sa) oscillator producing 6 fs pulses at a central wavelength of 800 nm with an energy of 2.5 nJ per pulse and a repetition rate of 80 MHz. A fraction at a wavelength of 1030 ± 2 nm of the broad-band oscillator emission was used to seed the OPCPA pump channel. The 1030 nm seed pulses with an energy of 2 nJ were stretched to a 2 ns duration and amplified in a two-stage amplifier. The first stage (regenerative amplifier s-Pulse HP, Amplitude Laser) and the second stage (Innoslab amplifier, Amphos 400 AMP), both operating at 100 Hz repetition rate,[62] increased the pulse energy to 1.4 and 27 mJ, respectively. After the amplification, the pulses were compressed to a duration of 1.2 ps with a compressor transmission of 60%. A 1 mJ fraction of the compressed pulse energy was frequency doubled and used to pump the first two OPCPA stages.

The 6 fs seed pulses at a central wavelength of 800 nm provided by the Ti:Sa oscillator were first stretched with the help of a 10 cm

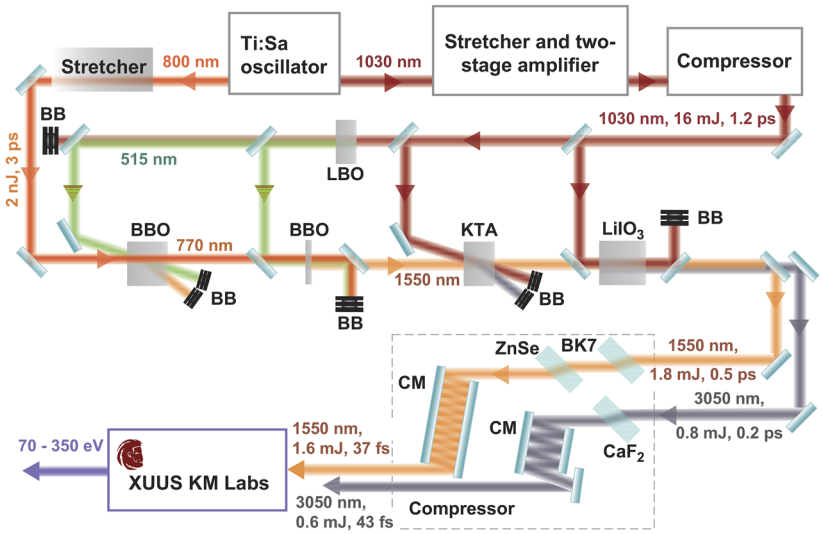

FIG. 1. Experimental schematic. A broadband Ti:Sa oscillator is used as a seed source for both the OPCPA itself and for the pump channel. The 6 fs pulses at a wavelength of 800 nm are stretched and used as seed for the four stage OPCPA, consisting of two BBO crystals followed by KTA and $LiIO_3$ stages. The pump channel is seeded with 1030 nm pulses and consists of a stretcher, two-stage amplifier, and compressor. Part of the pump radiation is converted to the second harmonic (SH) in an LBO crystal for pumping of BBO stages. BB stands for beam blocks. After the amplification, the pulses are compressed using CM and MD in ZnSe, BK7, and CaF_2. The pulses at a wavelength of 1550 nm are used for pumping the harmonic source.

BK7 slab to a duration of 3 ps full width at half maximum (FWHM), which is longer than the pump pulse duration. By changing the delay between the pump and the strongly stretched seed pulses, one could choose the central wavelength at which the amplification takes place.

In the first OPCPA stage, the pump (wavelength 515 nm) and the seed were interacting noncollinearly in a 3.9 mm thick type I beta-barium borate (BBO) crystal (θ = 24.3°). The noncollinear interaction with an angle of 2.4° allowed reaching high amplification while keeping a broad amplification spectrum. The next OPCPA stage was used for the difference frequency generation. The pump at a wavelength of 515 nm and the signal beam with a central wavelength shifted to 770 nm were interacting collinearly in order to avoid the angular chirp of the idler wave. In order to maintain the broad spectral width, a much shorter (0.6 mm) type I BBO crystal was used. The idler pulses of the second stage at a central wavelength of 1550 nm were amplified in the third OPCPA stage. A 3 mm thick type II KTA crystal (θ = 48.6°) was pumped by the pulses at a wavelength of 1030 nm in the noncollinear geometry (a noncollinear angle of 4.2°), providing high amplification in a wide spectrum. In the fourth and last OPCPA stage, pumped by the 1030 nm pulses, the radiation at a wavelength of 1550 nm (signal wave) was further amplified up to an energy of 1.8 mJ per pulse. For this purpose, a 4.5 mm thick type I $LiIO_3$ crystal was chosen because of its wide amplification bandwidth for a collinear interaction. The energy of the idler pulses at a wavelength of 3050 nm reached 0.8 mJ.

For the compression of both signal and idler pulses, combinations of material dispersion (MD) and chirped mirror (CM) dispersion were employed (Fig. 1). Such a combination allows better compensation of the second and third order dispersion and the possibility of dispersion fine-tuning. The pulse durations were determined using frequency-resolved optical gating (FROG).[63] An example of the measured and retrieved second-harmonic-generation (SHG) FROG traces for the signal pulse is shown in Figs. 2(a) and 2(b). The retrieved pulse [Fig. 2(c)] had a duration of 37 fs. The retrieved spectrum was in qualitative agreement with the independently measured one [Fig. 2(d)]. The pulse energy after the compression was 1.6 mJ. The duration of the compressed idler pulses was found to be 43 fs using third-harmonic-generation FROG. The energy of the compressed pulses was 0.6 mJ.

For the HHG generation, a specially adapted "XUUS" source from KM Labs (USA) was used.[64] The signal beam at a wavelength of 1550 nm was coupled into HCW using a 300 mm focal length CaF_2 lens (Fig. 3). The HCW with an inner diameter of 100 μm and a length of 10 mm was filled with argon, neon, or helium. For the optimum matching of the beam and the EH_{11} mode of the HCW, the beam waist diameter at $1/e^2$ was set to 64 μm. The inset in Fig. 3 shows the beam energy distribution in the focal plane of the lens. The gas at a pressure of up to 30 bars was injected through a hole in the middle of the HCW (Fig. 3) and evacuated on both sides with four roughing pumps.

The emitted radiation from the HCW was filtered with the help of a 200 nm Ti foil and recorded using a McPherson model 251MX flat field spectrometer[65] with a Greateyes (GE 2048 515 B1 UV1) charge-coupled device (CCD) camera (Fig. 3). The spectrometer chamber was pumped out with an additional vacuum pump down

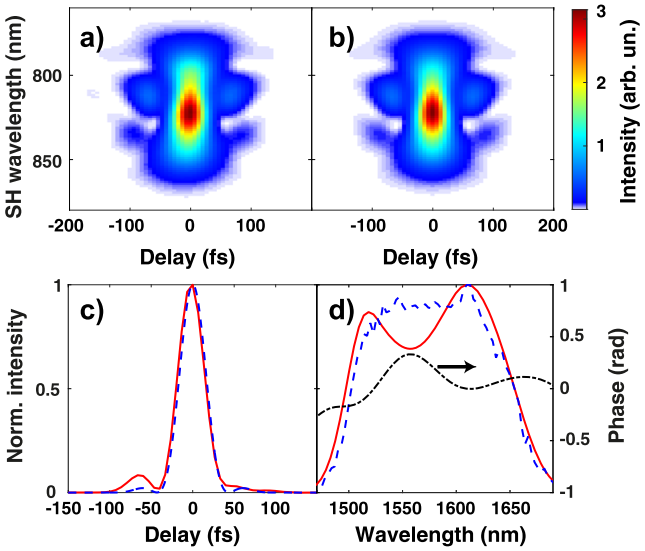

FIG. 2. Measured (a) and retrieved (b) SHG FROG traces of the pulses at a central wavelengths of 1550 nm. The retrieved pulse shape (37 fs FWHM) and spectrum are shown with red solid lines in panels (c) and (d), respectively. The blue dashed lines in (c) and (d) represent correspondingly the bandwidth limited pulse (35 fs FWHM) and the independently measured spectrum. The black dashed-dotted line in (d) shows the retrieved spectral phase.

to the pressure of 10^{-5}–10^{-3} mbar depending on the experimental conditions. The spectrometer was equipped with a pair of grazing incidence gratings on concave spherical substrates. The lower photon energy grating (LEG) with 1200 groves/mm and the higher photon energy grating (HEG) with 2400 groves/mm had nominal wavelength ranges of about 5–20 nm (250–60 eV) and about 1–6 nm (1240–200 eV). The reference spectra for both gratings can be found in Ref. 65. We have additionally checked the spectrometer calibration using a McPerson soft x-ray source 642.[66]

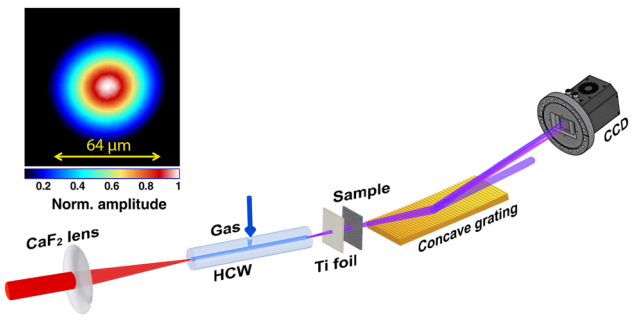

FIG. 3. Beam at a wavelength of 1550 nm is focused at the entrance of the HCW using a CaF_2 lens. The noble gas (Ar, Ne, or He) is injected through a small hole in the center of the HCW. The emission at the output of the HCW is filtered with a Ti foil and can be used for the XAS of a sample. The transmitted radiation is spectrally resolved with the help of a concave grating and recorded using a back-side illuminated CCD camera. Inset: energy distribution in the focal plane of the CaF_2 lens.

III. SWITCHING TO THE NONADIABATIC REGIME

Due to a constant gas flow through the HCW, a gas density drop is expected along the waveguide axis. Figure 4 (top panel) shows the density distribution along the axis calculated using Autodesk CFD (Computational Fluid Dynamics) software. Below we estimate the influence of this gradient on reaching the phase matched harmonic emission.

The wave vector mismatch Δk between the q-th harmonic and the corresponding polarization wave induced by the pump can be expressed as (see, e.g., Refs. 39, 51, and 67)

$$\Delta k = -q\frac{2\pi}{\lambda_L}(n_L - 1)(1-\eta)p + qN_a r_e \lambda_L \eta p + q\frac{u_{nm}^2 \lambda_L}{4\pi a^2}, \quad (1)$$

where n_L is the refractive index of the gas at the pump wavelength λ_L, η is the ionization fraction of the gas, N_a is the number density of atoms, r_e is the classical electron radius, u_{mn} is the capillary mode factor, and a is the capillary radius. Both n_L and N_a are taken at the pressure of 1 bar, and p is the gas pressure in bar. The factor $1-\eta$ takes into account the reduction of neutral atoms due to ionization. In (1) we have neglected the nonlinear refractive index of the gas.

The phase matching pressure tolerance is given by $\Delta p = \Delta k_{\mathrm{FWHM}}(d\Delta k/dp)^{-1}$. Above Δk_{FWHM} corresponds to the full width at half maximum of harmonic intensity as a function of Δk and satisfies the condition $\Delta k_{\mathrm{FWHM}} = 5.56/L$,[68] where L is the interaction (HCW) length. In the adiabatic regime with $\eta \approx 0$, one gets

$$\Delta p(\eta = 0) = \frac{5.56}{2\pi}\frac{1}{n_L - 1}\frac{\lambda_q}{L}, \quad (2)$$

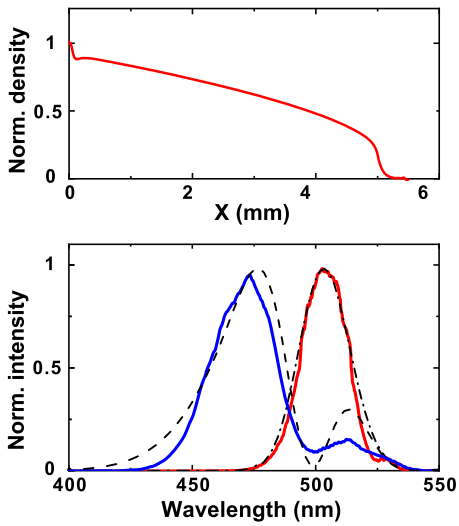

FIG. 4. Top panel: calculated gas density distribution along the axis of the HCW (X-axis). The distribution is symmetric with respect to the middle of the waveguide ($X = 0$). Bottom panel: measured (solid lines) and calculated (dashed and dashed-dotted lines) third harmonic spectra at the output of a He-filled HCW. The pump intensity was about 5×10^{14} W/cm^2. Red solid and black dashed-dotted lines correspond to a low He pressure. Blue solid and black dashed lines represent the spectra for a high He pressure.

above $\Delta p(\eta = 0)$ is the pressure tolerance in the adiabatic regime, and λ_q is the wavelength of the q-th harmonic. Simple estimations show that for harmonics with about 1 keV photon energy using $\lambda_L = 1550$ nm and $L = 1$ cm $\Delta p(\eta = 0)$ lies in the millibar range and no phase matching along the HCW is possible.

At higher intensities with the developing ionization, phase matching can be achieved for the fraction of a pump pulse because of the time dependent η (nonadiabatic or time gated regime[37,46,55,60]). However, the pressure tolerance can be sufficiently increased. Indeed, it follows from (1) that

$$\Delta p(\eta) = \frac{\Delta p(\eta = 0)}{1 - \eta/\eta_{cr}}, \quad (3)$$

where $\Delta p(\eta)$ is the pressure tolerance in the nonadiabatic regime and η_{cr} is the critical ionization fraction, starting from which the phase matching is no longer possible ($\eta_{cr} = [\lambda_L^2 N_a r_e/(2\pi(n_L - 1)) + 1]^{-1}$[39,52]).

The possibility of switching to the nonadiabatic regime in our experiments was checked for helium because it has the highest ionization potential. The ionization onset was monitored by measuring the blue shift of the spectrum of the third harmonic at the HCW output using a compact Ocean Optics USB spectrometer (Fig. 4, bottom panel). The pump intensity was about 5×10^{14} W/cm^2. At low He input pressures (<100 mbar), the generated electron density is too low, and no shift is observed (red solid curve). At 4 bars, the blue shift $\Delta\lambda_{3\omega}$ of about 25 nm was measured. Assuming the ratio of the fundamental shift $\Delta\lambda_\omega$ to that of the third harmonic to be about 2, as our simulations show, one gets $\Delta\lambda_\omega \approx 50$ nm. This shift corresponds to the electron production rate of $d\langle n_e\rangle/dt \approx 10^{15}$ cm^{-3} fs^{-1}, where the angle brackets indicate averaging along the HCW. Dividing this rate over $N_a\langle p\rangle$ one gets $d\eta/dt \approx 2 \times 10^{-5}$ fs^{-1}. At this rate the ionization fraction η can approach η_{cr} (which is about 10^{-3}) within the pulse duration, and according to (3) a larger pressure tolerance can be achieved. The necessary ionization fraction could be easily reached in Ar and Ne due to their lower ionization potential.

IV. HIGH HARMONIC GENERATION

Figure 5 shows the harmonic spectra generated in the nonadiabatic regime using Ar, Ne, and He. Altogether, the spectra cover the range from about 70 to about 350 eV. For maximum harmonic emission, the pressures and pump energies were 1.5 bars and 0.3 mJ for Ar, 3.7 bars and 0.7 mJ for Ne, and 9.3 bars and 0.8 mJ for He. Furthermore, we have increased the pulse duration to 54 fs in order to avoid self-focusing in ZnSe plates used for the pulse compression (see Fig. 1) and reach 80% coupling efficiency to the HCW. The photon numbers N_{ph} as a function of photon energy E were calculated from the corresponding counts of the CCD camera $N_c(E)$ according to

$$N_{ph}(E) = \frac{1}{T_G T_S}\frac{3.66\ \mathrm{eV}}{E}\frac{1}{\eta\kappa}N_c(E), \quad (4)$$

where T_G is the grating efficiency,[65] T_S is the spectrometer slit transmission, 3.66 eV is the average photon energy for producing a charge pair in silicon,[69] and η and κ are the quantum efficiency and gain of the CCD camera, respectively.[70] The photon fluxes for the 100 Hz repetition rate at the HCW output were evaluated from Fig. 5, taking into account the Ti foil and residual gas transmission. Thus, at

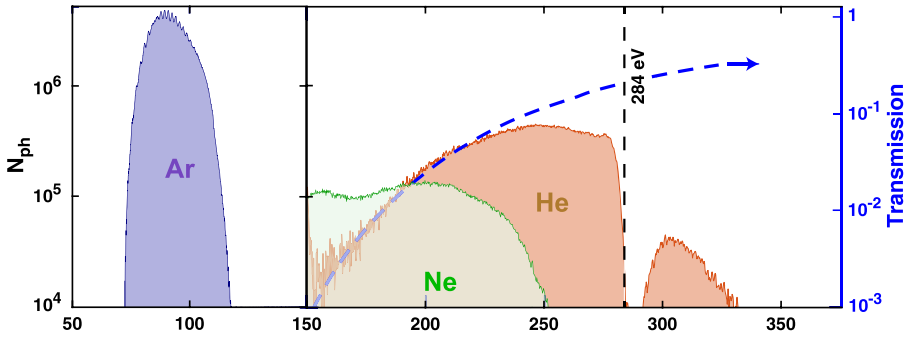

FIG. 5. Spectra of harmonics in Ar, Ne, and He taken in 5 min using the 1550 nm fundamental wavelength. N_{ph} represents the number of photons reaching the spectrometer slit within this acquisition time. In the case of Ar, the spectrum was recorded using the LEG, while for Ne and He, the HEG was used. The spectrum for Ne is limited on the left by the wavelength range of the spectrometer, which was calibrated to match the HHG in He. The pump radiation and lower harmonics were cut using a 200 nm thick Ti foil. The dashed blue line corresponds to the transmission of a 3 mm path in He at 5 bars and the Ti foil.

93 eV for Ar, 214 eV for Ne, and 270 eV for He, one gets fluxes of 10^7, 10^4, and 10^5 ph/s, respectively, integrated within the 1% bandwidth of the central photon energy.

The high energy cutoffs of the spectra follow the well-known low $\hbar\omega = I_p + 3.17U_p$[71] with the ponderomotive potential $U_p = 9.33 \times 10^{14} I_L \lambda_L^2$, where I_p and I_L are the gas ionization potential and laser intensity, respectively. The gap at about 284 eV in the case of He corresponds to the carbon K-edge and is due to the carbon contamination of the spectrometer.

The decay on the low energy side of the spectra is due to the absorption in the gas and in the Ti foil.[72,73] The dashed blue line in Fig. 5 shows the calculated transmission of He together with the foil. The He pressure was assumed to be 5 bars, which is the average pressure at the end of the capillary according to Fig. 4. The path length in He was taken to be 3 mm, corresponding to the best match to the measured spectrum. The good agreement indicates that despite a considerable pressure gradient in the HCW (Fig. 4, left panel), switching to the nonadiabatic regime allows an effective HHG length of several millimeters.

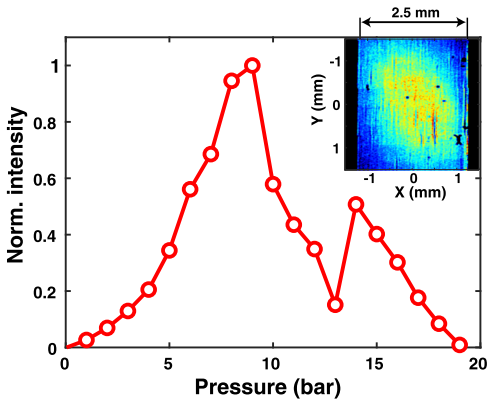

FIG. 6. Pressure dependence of the HHG intensity in He. Inset: spatial distribution of the harmonic emission at the position of the entrance slit of the spectrometer.

The pressure dependence of the intensity of the harmonic emission for the He-filled HCW is shown in Fig. 6. The quadratic growth of the intensity and saturation at a certain "optimum" pressure indicates the onset of the phase matched HHG. The shape of the harmonic beam at the entrance slit of the spectrometer can be evaluated from its image (see inset to Fig. 6) recorded with the CCD-camera using HCW filled with He. The image was taken in the zeroth diffraction order of the spectrometer grating with the slit widely open (2.5 mm width). It can be seen that the harmonic beam is slightly elliptic with vertical and horizontal sizes of about 2 mm FWHM. The image in Fig. 6 was corrected for spectrometer astigmatism. For the correction, the amount of astigmatism in the zeroth order was measured with the help of a helium–neon laser beam.

V. NEAR EDGE X-RAY ABSORPTION FINE STRUCTURE (NEXAFS)

The generated harmonic spectra allow XAS measurements on carbon and boron K-edges. In our experiments, we have focused on the boron edge, which has been shown to be very informative in several boron compounds.[74] HHG from HCW filled with He was used. On the one hand, it was because of lower photon flux with Ne, which we attribute to reabsorption of harmonics at a relatively high gas pressure. On the other hand, the dip in the spectrum at the position of the carbon K-edge, which was observed using He, could be used for better spectrometer calibration. A set of two samples with different boron configurations was placed in the harmonic beam, and the transmitted spectrum was measured with our spectrometer described above (see Fig. 3). A vacuum filter wheel was used as a sample holder and allowed a rapid exchange of them without breaking the vacuum. Since the holder was placed close to the spectrometer entrance slit, the size and shape of the x-ray beam on the samples were approximately the same as in Fig. 6. The first studied sample was a 100 nm thick boron foil, supported by a nickel mesh (Lebow Co.). The second one was a 5 × 5 mm^2 stack of hBN monolayers with a total thickness of 96 nm. The stack was prepared following a fabrication protocol described in detail in Ref. 75, with the modification of substituting the APS solution for 10% nitric acid. The sample was supported by a Si_3N_4 substrate with a thickness of 200 nm.

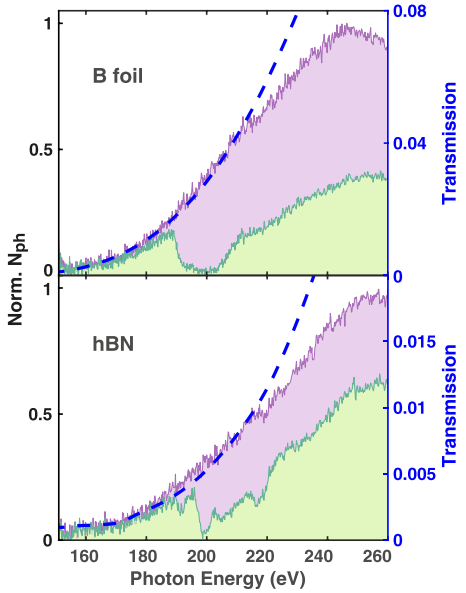

FIG. 7. Comparison of the transmission spectra (green-filled areas) and reference harmonic spectra (violet-filled areas). The samples were a boron foil (top) and an hBN sample (bottom). In the top panel, the dashed blue line corresponds to absorption in 200 nm Ti foil and a path of 3 mm in He at a pressure of 5 bars (top). In the bottom panel, additionally, a 200 mm Si_3N_4 substrate is taken into account, and the best fit is achieved with a 2 mm path.

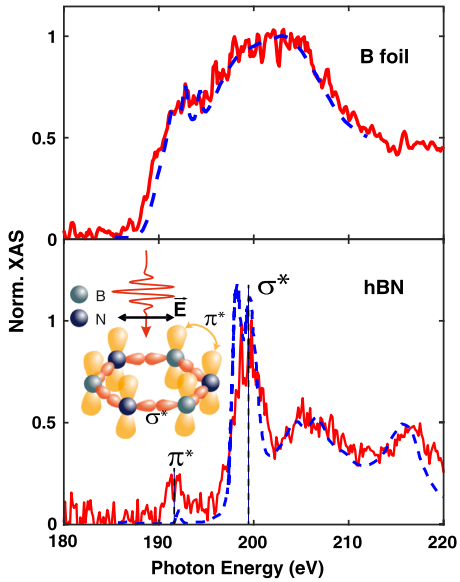

FIG. 8. XAS for a boron foil (top panel) and a hBN (bottom panel). The red solid lines represent the absorption spectra calculated from those shown in Fig. 7. The blue dashed lines correspond to the measurements [top panel, reproduced with permission from Jiménez *et al.*, J. Electron Spectrosc. Relat. Phenom. **101–103**, 611 (1999). Copyright 1999 Elsevier Science B.V. All rights reserved] and [bottom panel, reproduced with permission from Wang *et al.*, Nanoscale **7**, 1718 (2015). Copyright 2015 the Royal Society of Chemistry]. The vertical black dashed lines indicate the positions of the π^*- and most intense σ^*-resonance of hBN. The inset in the bottom panel illustrates schematically the orientation of the electric field of the pulse with respect to the π^* and σ^* orbitals in the 2D hBN layers.

Figure 7 shows the corresponding transmission spectra of the samples (in green) together with the reference HHG spectra (in violet), which were captured without the samples in the beam path. The spectra are normalized to the maxima of the corresponding reference. Each spectrum was obtained in a total time of 20–30 min. A clear difference in the transmitted spectra can be observed.

Figure 8 represents the retrieved XAS for the boron foil and the hBN sample. The retrieved spectrum of the boron foil (Fig. 8, top panel) is in good agreement with the one recorded by Jiménez *et al.*[74] using polycrystalline boron at the Stanford Synchrotron Radiation Lightsource. Both spectra show a step starting with the edge jump around 190 eV and going up to around 195 eV, followed by a broad feature of higher amplitude up to 210 eV.

The retrieved NEXAFS of hBN agrees well with the measurements of the XAS fine structures by Wang *et al.*[76] The well-resolved spectral structure can be attributed to the known resonances of hBN. A spectral resolution of 2 eV was estimated by comparing the measured and the reference curves in Fig. 8, bottom. The peak at 192 eV is the π^* resonance, while the features at 198, 199, 204, 206, and 213 eV are due to different σ^* resonances.[76] The relatively weak contribution due to the π^* resonance in our measurements can be attributed (as well as in Ref. 76) to the fact that the HHG beam was nearly orthogonal to the sample, which is a 2D material. In this case, the electric field, which lies predominantly in the plane of the hBN layers (see inset in Fig. 8), cannot effectively excite the π^* resonance because for the transition 1s–π^* the scalar product of the field and the corresponding matrix element of the dipole momentum is small.

The set-up provides synchronized laser and x-ray pulses, which may allow for carrying out time resolved experiments. These experiments require relatively long measuring times, which is possible with the present set-up. Several hours of accumulation without additional adjustments were demonstrated using an active stabilization system of the pump beam employed in the XUUS source.[77]

VI. CONCLUSIONS

In conclusion, we have presented a table-top soft x-ray source for XAS experiments with a 100 Hz repetition rate. The source is based on HHG in a noble-gas-filled HCW pumped with pulses at a wavelength of 1550 nm. It produces broadband spectra with photon energies from 70 to 350 eV. Because of a small diameter HCW (100 μm), the x-ray emission is generated by pump pulses with energies below 1 mJ. Despite a substantial pressure gradient along the HCW, switching to the nonadiabatic regime allows reaching coherence lengths of the HHG of several millimeters. A longer (1 cm) HCW allows moderate gas consumption and pump rates of the vacuum pumps. With the He filled HCW photon fluxes of about 10^5 ph/s at an energy of 270 eV in a fractional bandwidth of 1% are reached. The characteristics and the overall performance of the setup have been demonstrated with NEXAFS measurements on the B K-edge with a 2 eV energy resolution and 20–30 min averaging per recorded spectrum for a boron foil and a hBN sample.

The source provides opportunities for femtosecond time-resolved XAS experiments. Our measurements (Fig. 8) demonstrate

a rich, fine structure in the K edge absorption spectrum of B, which is well resolved. The analysis of pump-induced changes in x-ray absorption spectra at this absorption edge seems very promising, in particular if it can be combined with polarization selectivity, as the comparison of the spectra obtained for bulk B and h-BN indicates.

The reported photon flux at 270 eV is comparable to or higher than that reported for most HHG sources (e.g., Refs. 29, 33, 57, and 59). Two orders of magnitude higher fluxes at about 300 eV have been reported at 1 kHz repetition rates using higher pump energy[54] or sub-2-cycle pump pulses.[30] The planned increase in the repetition rate to 10–15 kHz[62] will allow us to reach this level and strongly decrease the acquisition time per absorption spectrum. The higher photon energy of the HHG source can be achieved by switching to the idler pulses with a central wavelength of 3050 nm (see Fig. 1). Reaching the necessary level of ionization for the nonadiabatic phase matching will be possible with these pulses after a planned energy upgrade of the set-up.

ACKNOWLEDGMENTS

We thank Margaret Murnane and Henry Kapteyn for fruitful discussions. We acknowledge the financial support by the Deutsche Forschungsgemeinschaft through SFB 1242 (Project No. 278162697) and the Bundesministerium für Bildung und Forschung through Project No. 05K19PG1.

AUTHOR DECLARATIONS

Conflict of Interest

The authors have no conflicts to disclose.

Author Contributions

All authors provided critical feedback and helped shape the research, analysis, and manuscript.

O. A. Naranjo-Montoya: Data curation (equal); Investigation (equal); Resources (equal). **M. Bridger**: Resources (equal). **R. Bhar**: Resources (equal). **L. Kalkhoff**: Resources (equal). **M. Schleberger**: Resources (equal). **H. Wende**: Conceptualization (equal); Funding acquisition (equal); Writing – review & editing (equal). **A. Tarasevitch**: Data curation (equal); Funding acquisition (equal); Investigation (equal); Methodology (equal); Resources (equal); Software (equal); Writing – original draft (equal); Writing – review & editing (equal). **U. Bovensiepen**: Conceptualization (equal); Funding acquisition (equal); Supervision (equal); Writing – original draft (equal); Writing – review & editing (equal).

DATA AVAILABILITY

The data that support the findings of this study are available from the corresponding author upon reasonable request.

REFERENCES

[1] F. de Groot, Chem. Rev. **101**, 1779 (2001).
[2] J. Stöhr, *NEXAFS Spectroscopy*, 1st ed. (Springer, Berlin, Heidelberg, 1992).
[3] P. A. Lee, P. H. Citrin, P. Eisenberger, and B. M. Kincaid, Rev. Mod. Phys. **53**, 769 (1981).
[4] L. J. P. Ament, M. van Veenendaal, T. P. Devereaux, J. P. Hill, and J. van den Brink, Rev. Mod. Phys. **83**, 705 (2011).
[5] F. Gel'mukhanov, M. Odelius, S. P. Polyutov, A. Föhlisch, and V. Kimberg, Rev. Mod. Phys. **93**, 035001 (2021).
[6] *X-Ray Absorption Spectroscopy of Semiconductors*, 1st ed., edited by C. S. Schnohr and M. C. Ridgway (Springer, Berlin, Heidelberg, 2014).
[7] G. van der Laan and A. I. Figueroa, Coord. Chem. Rev. **277–278**, 95 (2014).
[8] *Magnetic Measurement Techniques for Materials Characterization*, 1st ed., edited by V. Franco and B. Dodrill (Springer, Cham, 2021).
[9] The Surface Science Society of Japan (Ed.), *Compendium of Surface and Interface Analysis*, 1st ed. (Springer, Singapore, 2018).
[10] J. E. Penner-Hahn, Coord. Chem. Rev. **190–192**, 1101 (1999).
[11] G. E. Cutsail III and S. DeBeer, ACS Catal. **12**, 5864 (2022).
[12] J. Yano and V. K. Yachandra, Photosynth. Res. **102**, 241 (2009).
[13] A. Guilherme Buzanich, X-Ray Spectrom. **51**, 294 (2022).
[14] F. Farges and M. Cotte, in *X-Ray Absorption and X-Ray Emission Spectroscopy: Theory and Applications*, edited by J. A. V. Bokhoven and C. Lamberti (Wiley Online Library, 2016).
[15] M. Cotte, J. Susini, J. Dik, and K. Janssens, Acc. Chem. Res. **43**, 705 (2010).
[16] M. Siegbahn, Ann. Phys. **364**, 56 (1919).
[17] D. E. Sayers, E. A. Stern, and F. W. Lytle, Phys. Rev. Lett. **27**, 1204 (1971).
[18] W. Malzer, C. Schlesiger, and B. Kanngießer, Spectrochim. Acta, Part B **177**, 106101 (2021).
[19] H. Öström, H. Öberg, H. Xin, J. LaRue, M. Beye, M. Dell'Angela, J. Gladh, M. L. Ng, J. A. Sellberg, S. Kaya, G. Mercurio, D. Nordlund, M. Hantschmann, F. Hieke, D. Kühn, W. F. Schlotter, G. L. Dakovski, J. J. Turner, M. P. Minitti, A. Mitra, S. P. Moeller, A. Föhlisch, M. Wolf, W. Wurth, M. Persson, J. K. Nørskov, F. Abild-Pedersen, H. Ogasawara, L. G. M. Pettersson, and A. Nilsson, Science **347**, 978 (2015).
[20] D. R. Baykusheva, H. Jang, A. A. Husain, S. Lee, S. F. R. TenHuisen, P. Zhou, S. Park, H. Kim, J.-K. Kim, H.-D. Kim, M. Kim, S.-Y. Park, P. Abbamonte, B. J. Kim, G. D. Gu, Y. Wang, and M. Mitrano, Phys. Rev. X **12**, 011013 (2022).
[21] L. Le Guyader, A. Eschenlohr, M. Beye, W. Schlotter, F. Döring, C. Carinan, D. Hickin, N. Agarwal, C. Boeglin, U. Bovensiepen *et al.*, J. Synchrotron Radiat. **30**, 284 (2023).
[22] T. Lojewski, M. F. Elhanoty, L. L. Guyader, O. Grånäs, N. Agarwal, C. Boeglin, R. Carley, A. Castoldi, C. David, C. Deiter, F. Döring, R. Engel, F. Erdinger, H. Fangohr, C. Fiorini, P. Fischer, N. Gerasimova, R. Gort, F. deGroot, K. Hansen, S. Hauf, D. Hickin, M. Izquierdo, B. E. V. Kuiken, Y. Kvashnin, C.-H. Lambert, D. Lomidze, S. Maffessanti, L. Mercadier, G. Mercurio, P. S. Miedema, K. Ollefs, M. Pace, M. Porro, J. Rezvani, B. Rösner, N. Rothenbach, A. Samartsev, A. Scherz, J. Schlappa, C. Stamm, M. Teichmann, P. Thunström, M. Turcato, A. Yaroslavtsev, J. Zhu, M. Beye, H. Wende, U. Bovensiepen, O. Eriksson, and A. Eschenlohr, Mater. Res. Lett. **11**, 655 (2023).
[23] M. Chergui, M. Beye, S. Mukamel, C. Svetina, and C. Masciovecchio, Nat. Rev. Phys. **5**, 578 (2023).
[24] I. Matsuda and R. Arafune, *Nonlinear X-Ray Spectroscopy for Materials, Science Springer Series in Optical Sciences Vol. 246* (Springer, Singapore, 2023).
[25] A. Jonas, H. Stiel, L. Glöggler, D. Dahm, K. Dammer, B. Kanngießer, and I. Mantouvalou, Opt. Express **27**, 36524 (2019).
[26] M. Borchert, J. Braenzel, R. Gnewkow, L. Lunin, T. Sidiropoulos, J. Tümmler, I. Will, T. Noll, O. Reichel, D. Rohloff, A. Erko, T. Krist, C. von Korff Schmising, B. Pfau, S. Eisebitt *et al.*, Rev. Sci. Instrum. **94**, 063102 (2023).
[27] D. Popmintchev, B. R. Galloway, M.-C. Chen, F. Dollar, C. A. Mancuso, A. Hankla, L. Miaja-Avila, G. O'Neil, J. M. Shaw, G. Fan, S. Ališauskas, G. Andriukaitis, T. Balčiunas, O. D. Mücke, A. Pugzlys, A. Baltuška, H. C. Kapteyn, T. Popmintchev, and M. M. Murnane, Phys. Rev. Lett. **120**, 093002 (2018).
[28] G. Fan, K. Légaré, V. Cardin, X. Xie, R. Safaei, E. Kaksis, G. Andriukaitis, A. Pugžlys, B. E. Schmidt, J. P. Wolf, M. Hehn, G. Malinowski, B. Vodungbo, E. Jal, J. Lüning, N. Jaouen, G. Giovannetti, F. Calegari, Z. Tao, A. Baltuška, F. Légaré, and T. Balčiūnas, Optica **9**, 399 (2022).
[29] E. J. Takahashi, T. Kanai, K. L. Ishikawa, Y. Nabekawa, and K. Midorikawa, Phys. Rev. Lett. **101**, 253901 (2008).

[30]S. L. Cousin, F. Silva, S. Teichmann, M. Hemmer, B. Buades, and J. Biegert, Opt. Lett. **39**, 5383 (2014).
[31]Y. Pertot, C. Schmidt, M. Matthews, A. Chauvet, M. Huppert, V. Svoboda, A. von Conta, A. Tehlar, D. Baykusheva, J.-P. Wolf, and H. J. Wörner, Science **355**, 264 (2017).
[32]A. R. Attar, A. Bhattacherjee, C. D. Pemmaraju, K. Schnorr, K. D. Closser, D. Prendergast, and S. R. Leone, Science **356**, 54 (2017).
[33]C. Kleine, M. Ekimova, G. Goldsztejn, S. Raabe, C. Strüber, J. Ludwig, S. Yarlagadda, S. Eisebitt, M. J. J. Vrakking, T. Elsaesser, E. T. J. Nibbering, and A. Rouzée, J. Phys. Chem. Lett. **10**, 52 (2019).
[34]Z. Chang, A. Rundquist, H. Wang, M. Murnane, and H. Kapteyn, Phys. Rev. Lett. **79**, 2967 (1997).
[35]C. Spielmann, N. Burnett, S. Sartania, R. Koppitsch, M. Schnürer, C. Kan, M. Lenzner, P. Wobrauschek, and F. Krausz, Science **278**, 661 (1997).
[36]C. Joachain, M. Dörr, and N. Kylstra, Adv. At., Mol., Opt. Phys. **42**, 225 (2000).
[37]T. Brabec and F. Krausz, Rev. Mod. Phys. **72**, 545 (2000).
[38]E. Gibson, A. Paul, N. Wagner, R. Tobey, D. Gaudiosi, S. Backus, I. Christov, A. Aquila, E. Gullikson, D. Attwood, M. Murnane, and H. Kapteyn, Science **302**, 95 (2003).
[39]T. Popmintchev, M.-C. Chen, A. Bahabad, M. Gerrity, P. Sidorenko, O. Cohen, I. Christov, M. Murnane, and H. Kapteyn, Proc. Natl. Acad. Sci. U. S. A. **106**, 10516 (2009).
[40]M. Chen, P. Arpin, T. Popmintchev, M. Gerrity, B. Zhang, M. Seaberg, D. Popmintchev, M. Murnane, and H. Kapteyn, Phys. Rev. Lett. **105**, 173901 (2010).
[41]N. Ishii, K. Kaneshima, T. Kanai, S. Watanabe, and J. Itatani, J. Opt. **20**, 014003 (2018).
[42]P. M. Kraus, M. Zürch, S. K. Cushing, D. M. Neumark, and S. R. Leone, Nat. Rev. Chem. **2**, 82 (2018).
[43]K. S. Zinchenko, F. Ardana-Lamas, V. U. Lanfaloni, N. Monahan, I. Seidu, M. S. Schuurman, S. P. Neville, and H. J. Wörner, Struct. Dyn. **10**, 064303 (2023).
[44]T. P. H. Sidiropoulos, N. Di Palo, D. E. Rivas, S. Severino, M. Reduzzi, B. Nandy, B. Bauerhenne, S. Krylow, T. Vasileiadis, T. Danz, P. Elliott, S. Sharma, K. Dewhurst, C. Ropers, Y. Joly, M. E. Garcia, M. Wolf, R. Ernstorfer, and J. Biegert, Phys. Rev. X **11**, 041060 (2021).
[45]T. Popmintchev, M.-C. Chen, D. Popmintchev, P. Arpin, S. Brown, S. Ališauskas, G. Andriukaitis, T. Balčiunas, O. Mücke, A. Pugžlys, A. Baltuška, B. Shim, S. Schrauth, A. Gaeta, C. Hernández-García, L. Plaja, A. Becker, A. Jaron-Becker, M. Murnane, and H. Kapteyn, Science **336**, 1287 (2012).
[46]M. Geissler, G. Tempea, and T. Brabec, Phys. Rev. A **62**, 033817 (2000).
[47]G. Tempea, M. Geissler, M. Schnürer, and T. Brabec, Phys. Rev. Lett. **84**, 4329 (2000).
[48]C. M. Heyl, J. Güdde, A. L'Huillier, and U. Höfer, J. Phys. B: At., Mol. Opt. Phys. **45**, 074020 (2012).
[49]Y. Tao, S. Goh, H. Bastiaens, P. van der Slot, S. Biedron, S. Milton, and K. Boller, Opt. Express **25**, 3621 (2017).
[50]J. Pupeikis, P.-A. Chevreuil, N. Bigler, L. Gallmann, C. R. Phillips, and U. Keller, Optica **7**, 168 (2020).
[51]A. Rundquist, C. G. Durfee III, Z. Chang, C. Herne, S. Mackus, M. Murnane, and H. Kapteyn, Science **280**, 1412 (1998).
[52]C. G. Durfee III, A. Rundquist, C. Herne, M. Murnane, and H. Kapteyn, Phys. Rev. Lett. **83**, 2187 (1999).
[53]M.-C. Chen, C. Mancusoa, C. Hernández-García, F. Dollara, B. Gallowaya, D. Popmintcheva, P.-C. Huangb, B. Walkerd, L. Plajac, A. A. Jaroń-Becker, A. Becker, M. Murnane, H. Kapteyn, and T. Popmintchev, Proc. Natl. Acad. Sci. U. S. A. **111**, E2361 (2014).
[54]C. Ding, W. Xiong, T. Fan, D. D. Hickstein, T. Popmintchev, X. Zhang, M. Walls, M. M. Murnane, and H. C. Kapteyn, Opt. Express **22**, 6194 (2014).
[55]C. Hernández-García, T. Popmintchev, M. Murnane, H. Kapteyn, L. Plaja, A. Becker, and A. Jaron-Becker, New J. Phys. **18**, 073031 (2016).
[56]E. Constant, D. Garzella, P. Breger, E. Mével, C. Dorrer, C. Le Blanc, F. Salin, and P. Agostini, Phys. Rev. Lett. **82**, 1668 (1999).
[57]A. Johnson, D. Austin, D. Wood, C. Brahms, A. Gregory, K. Holzner, S. Jarosch, E. Larsen, S. Parker, C. Strüber, P. Ye, J. Tisch, and J. Marangos, Sci. Adv. **4**, 3761 (2018).
[58]D. S. Steingrube, T. Vockerodt, E. Schulz, U. Morgner, and M. Kovačev, Phys. Rev. A **80**, 043819 (2009).
[59]V. Cardin, B. E. Schmidt, N. Thiré, S. Beaulieu, V. Wanie, M. Negro, C. Vozzi, V. Tosa, and F. Légaré, J. Phys. B: At., Mol. Opt. Phys. **51**, 174004 (2018).
[60]S. C. Rae, K. Burnett, and J. Cooper, Phys. Rev. A **50**, 3438 (1994).
[61]M. Bridger, O. A. Naranjo-Montoya, A. Tarasevitch, and U. Bovensiepen, Opt. Express **27**, 31330 (2019).
[62]The configuration of the pump channel allows a maximum repetition rate of about 15 kHz for the pulse energy of 27 mJ, which corresponds to the maximum average power of about 400 W.
[63]R. Trebino, *Frequency-Resolved Optical Gating: The Measurement of Ultrashort Laser Pulses* (Springer, Boston, MA, 2000).
[64]See https://www.kmlabs.com/product/xuus for the information on the XUUS source.
[65]Parameters of the 251MX spectrometer can be found here: https://www.mcphersoninc.com/pdf/251MX.pdf.
[66]For information about the 642 soft x-ray source see https://mcphersoninc.com/pdf/642-SXR-source.pdf.
[67]A. Rundquist, "Phase-matched generation of coherent, ultrafast X-rays using high harmonics," Ph.D. thesis, Washington State University, 1998.
[68]The constant 5.56 comes from the FWHM of the function $\mathrm{sinc}^2(\Delta kL/2)$, which gives the Δk-dependence of the harmonic intensity.
[69]F. Scholze, H. Rabus, and G. Ulm, J. Appl. Phys. **84**, 2926 (1998).
[70]The GE 2048 515 B1 UV1 camera parameters are similar to those of an upgraded version ALEXs 2k512 BI UV1 and can be found here: https://greateyes.de/cameras/alex-high-performance-ccd-cameras/alexs-deep-cooling-ccd-spectroscopy/#ALEXS2K512BIUV1.
[71]P. B. Corkum, Phys. Rev. Lett. **71**, 1994 (1993).
[72]See https://henke.lbl.gov/optical_constants for the x-ray absorption data.
[73]M. Nagasaka, J. Synchrotron Radiat. **27**, 959 (2020).
[74]I. Jiménez, L. J. Terminello, F. J. Himpsel, M. Grush, and T. Callcot, J. Electron Spectrosc. Relat. Phenom. **101–103**, 611 (1999).
[75]L. Kalkhoff, S. Matschy, A. S. Meyer, L. Lasnig, N. Junker, M. Mittendorff, L. Breuer, and M. Schleberger, "Ultra-large polymer-free suspended graphene films," arXiv:2311.08137 [physics.app-ph] (2023).
[76]J. Wang, Z. Wang, H. Cho, M. J. Kim, T. K. Sham, and X. Sun, Nanoscale **7**, 1718 (2015).
[77]O. A. Naranjo-Montoya, "OPCPA-driven high harmonic generation for soft X-ray absorption spectroscopy," Ph.D. thesis, University of Duisburg-Essen, Duisburg, 2023.